Oxid Met (2011) 76:215–232
DOI 10.1007/s11085-011-9249-3

ORIGINAL PAPER

Oxidation of Advanced Zirconium Cladding Alloys in Steam at Temperatures in the Range of 600–1200 °C

Martin Steinbrück · Nóra Vér · Mirco Große

Received: 8 December 2010 / Revised: 14 March 2011 / Published online: 26 March 2011
© Springer Science+Business Media, LLC 2011

Abstract The oxidation kinetics of the classical pressurized water reactors (PWR) cladding alloy Zircaloy-4 have been extensively investigated over a wide temperature range from operational conditions to beyond design basis accident (BDBA) temperatures. In recent years, new cladding alloys optimized for longer operation and higher burn-up are used in Western light water reactors (LWR). This paper presents the results of thermo-gravimetric tests with Zircaloy-4 as the reference material, Duplex DX-D4, M5® (both AREVA), ZIRLO™ (Westinghouse), and the Russian E110 alloy. All materials were investigated in isothermal and transient tests in a thermal balance with steam furnace. Post-test analyses were performed by light-microscopy and neutron radiography for investigation of the hydrogen absorbed by the metal. Strong and varying differences (up to 800%) in oxidation kinetics between the alloys were found at up to 1000 °C, where the breakaway effect plays a role. Less but significant differences (ca. 30%) were observed at 1100 and 1200 °C. Generally, the M5® alloy revealed the lowest oxidation rate over the temperature range investigated whereas the behavior of the other alloys was considerably dependent on temperature. A strong correlation was found between oxide scale structure and amount of absorbed hydrogen.

Keywords High-temperature oxidation · Zirconium alloys · Cladding · Light water reactor · Nuclear safety

M. Steinbrück (✉) · M. Große
Karlsruhe Institute of Technology, Institute for Applied Materials,
P.O. Box 3640, 76021 Karlsruhe, Germany
e-mail: martin.steinbrueck@kit.edu

N. Vér
AEKI, Budapest, Hungary

List of symbols

ACM	Advanced cladding materials
DX-D4	AREVA duplex cladding
E110	Russian cladding alloy (Zr1Nb)
FZK	Forschungszentrum Karlsruhe
ISTC	International Science and Technology Center
KIT	Karlsruhe Institute of Technology
k_m	Rate constant
LOCA	Loss of coolant accident
LWR	Light water reactor
M5®	AREVA cladding alloy (Zr1Nb)
PWR	Pressurized Water Reactor
QUENCH	Research program on reflood of an overheated reactor core at KIT
RIA	Reactivity initiated accident
S	Surface area
SARNET	Severe accident network (EC Program)
STA	Simultaneous thermal analysis
TG	Thermo-gravimetry
VVER	Russian PWR reactor
ZIRLO™	Westinghouse cladding alloy (Zr1Nb1Sn)
Zry-4	Zircaloy-4 cladding alloy (Zr1Sn)
Δm	Mass gain

Introduction

Zirconium alloys are widely used in the nuclear and chemical industries because of their low neutron absorption and excellent mechanical and corrosion properties. Zircaloy-4 with approx. 1.5 wt% tin as the major alloying element is a classical zirconium alloy for nuclear applications. It is used for fuel cladding, control rod guide tubes, and grid spacers. A huge data base is available for this alloy regarding the oxidation kinetics in steam over a wide range of temperatures from operational conditions (~300 °C) up to temperatures expected for hypothetical severe accidents (>1800 °C)[1, 2] and references herein. The oxidation correlations of computer codes simulating accident scenarios today mainly rely on Zircaloy-4 data.

Meanwhile, new advanced cladding alloys have been developed for longer operation times in nuclear power plants and extended burn-up of the fuel elements. They are optimized regarding their corrosion behavior under operational conditions and were also tested for LOCA (loss-of- coolant accident) and RIA (reactivity-initiated accident) conditions by the manufacturers. However, there are only very limited data publicly available on the behavior of the new alloys under accident conditions, i.e., at temperatures above 800 °C.

Therefore, an experimental program has been launched at Karlsruhe Institute of Technology (KIT, formerly Forschungszentrum Karlsruhe, FZK) on the

investigation of the high-temperature properties of advanced cladding alloys with special emphasis on the oxidation kinetics in various atmospheres.

This paper summarizes the results of thermo-gravimetric (TG) experiments on the oxidation behavior of five different zirconium alloys in steam. Further oxidation experiments in steam have been conducted in a horizontal furnace [3]; and TG oxidation tests in oxygen [4] and air [5] have been performed recently. Large-scale bundle tests on the integral behavior of advanced cladding materials during high-temperature transients and reflood have been conducted in the frame of the QUENCH-ACM program at KIT [6].

Experimental Procedures

The following alloys have been investigated in this study: Duplex DX-D4, M5® (both from AREVA), ZIRLO™ (Westinghouse), E110 (Electrostal, Russia), and Zircaloy-4 as the reference material. M5® and E110 are niobium-bearing alloys (Zr–1Nb) whereas "Duplex DX-D4" stands for a low-tin duplex cladding material. It consists of Zircaloy-4 as the base material and an outer liner of 0.15 mm with less Sn, and more Fe and Cr compared to the base material. ZIRLO™ contains both niobium and tin (Zr–1Nb–1Sn). E110 is mainly used in Russian VVER reactors whereas the others are used in Western pressurized water reactors (PWRs).

Table 1 gives an overview of the content of the main alloying elements of the materials investigated in this study. All samples used were 20 mm long cladding tube segments with 7.73 mm inner diameter and 9.13 mm outer diameter for E110, 8.357 mm inner diameter and 9.5 mm outer diameter for ZIRLO™, and 9.3 mm inner diameter and 10.75 mm outer diameter for Zry-4, Duplex, and M5®. The segments were cut from longer tubes, deburred, ground, and cleaned in acetone. Oxidation took place on both sides; various attempts to exclude internal oxidation were not successful. This means, amongst others, that the results obtained for the Duplex cladding are mixed ones including oxidation of the external low-tin alloy and of the internal 1.5-wt% tin alloy.

All experiments presented here were conducted in a commercial thermal balance (Netzsch STA 409) with steam generator and special steam furnace coupled with a quadrupole mass spectrometer (Netzsch Aeolos). The latter was used for process control, mainly to check the purity and composition of the gas mixture. All tests were run in 5 g/h flowing steam. The construction of the furnace allowed working

Table 1 Composition of the alloys investigated, main alloying elements in wt%, balance: Zr

Alloy	Nb	Sn	Fe	Cr	O
Zry-4	–	1.5	0.2	0.1	0.14
D4	–	0.5	0.5	0.2	0.14
M5	1	–	0.05	0.02	0.14
E110	1	–	0.008	0.002	0.05
Zirlo	1	1	0.1	<0.01	0.11

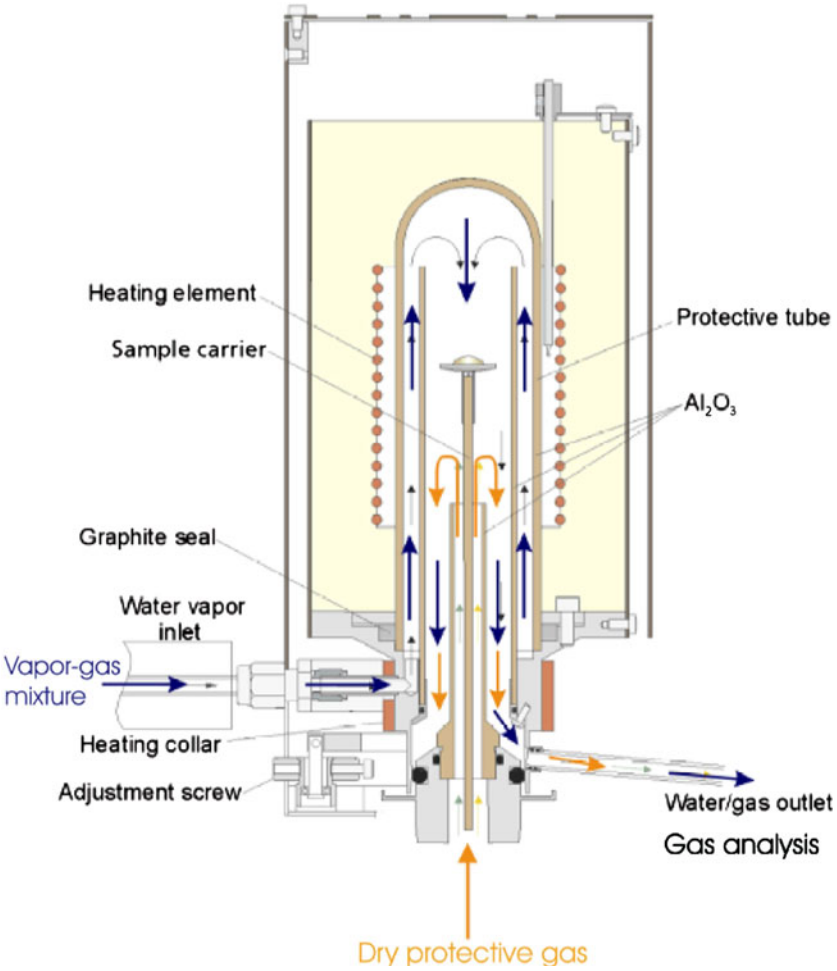

Fig. 1 Schematic of the steam furnace of the TG unit (Courtesy of NETZSCH-Gerätebau GmbH)

under a pure steam atmosphere (Fig. 1), although 5 l/h argon was injected in the balance volume as protective gas.

Isothermal tests have been performed between 600 and 1200 °C in 100 K steps with 48–1 h annealing time, respectively, resulting in a reasonable oxidation for metallographic examination. Transient tests were run with a heating rate of 5–40 K/min from 600 to 1200 °C. In isothermal tests, the specimens were heated in inert atmosphere (5 l/h Ar) to the desired temperature. After 10 min for temperature homogenization, 5 g/h steam were injected in the reaction tube to the end of the isothermal temperature plateau.

After the tests, one sample half was embedded in epoxy resin, ground, and polished for metallographic examinations by light microscopy. The other halves were used for determination of absorbed hydrogen by neutron radiography. The method is described in [7].

Experimental Results

Isothermal Tests in the Range of 600–1200 °C

The annealing time under oxidizing atmosphere was 48 h at 600 °C, 24 h at 700, 800, and 900 °C, 3 h at 1000 and 1100 °C, and 1 h at 1200 °C resulting in a partial cladding oxidation from 1 to 30 wt% corresponding to 35 wt% mass gain for complete oxidation to ZrO_2.

Figure 2 presents all thermo-gravimetric (TG) curves recorded during the isothermal experiments. At a first glance, the diagrams reveal a complex behavior at least up to 1000 °C. They show quite different appearances regarding slopes of curves, i.e., oxidation rates, and sequence of the five alloys from temperature to temperature. So, for example, ZIRLO™ shows the highest oxidation rate at 600, 700, and 1000 °C, an intermediate one at 800 and 900 °C, and is among the slowest at 1100 and 1200 °C.

Interestingly, the oxidation rates of the two niobium alloys E110 and M5® are quite different up to 1000 °C and almost identical at 1100 and 1200 °C. ZIRLO™ seems to be more similar to the tin-bearing alloys Zircaloy-4 and Duplex at lower temperatures, where breakaway plays a role, and corresponds to the niobium-bearing alloys M5® and E110 at higher temperatures. The oxidations of the two tin alloys Zry-4 and DX-D4 are closer to each other though with a persistent slightly slower rate of the low-tin D4 alloy. (The slightly higher oxidation rate of Duplex at 1200 °C is caused by more pronounced axial macro cracks.) The difference between the lowest and the highest oxidation rate is very strong (up to 800%) for temperatures of up to 1000 °C, and less, but still significant (about 30%) for 1100 and 1200 °C.

Furthermore, most of the TG curves (excluding M5®) up to 1000 °C show a more or less pronounced change in slope after a certain oxidation time, indicating changes in oxidation mechanisms. This change is rather abrupt for the tin alloys at most temperatures and more gradual for the niobium alloys and takes place at thicker oxide scales with increasing temperature. At 1100 and 1200 °C, no such transition was observed.

With increasing temperature, a raising initial rapid mass gain was observed due to a temporary temperature overshooting at begin of steam injection. This had to be taken into account, e.g., during calculation of kinetic rate constants.

The post-test appearance of specimens of the test series at 700 and 1000 °C is exemplified in Fig. 3. The samples differ in color and in the degree of degradation. Spalled oxide scales are clearly visible for the E110 and ZIRLO™ specimens at 1000 °C (and were also seen at 800 and 900 °C), indicating most pronounced breakaway oxidation. The Zircaloy-4 and Duplex specimens reveal crack networks. The M5® specimens show the lowest degradation over the whole temperature range.

Strong flaking at the edges was seen for the Zry-4 and Duplex specimens after the 800 °C tests, which correlates with the pronounced mass increase after 8–9 h. Both tests were repeated with carefully prepared specimens with the same result. For all other tests, no such edge effects were found. The specimens at 1100 and 1200 °C were almost completely oxidized resulting in the formation of axial cracks.

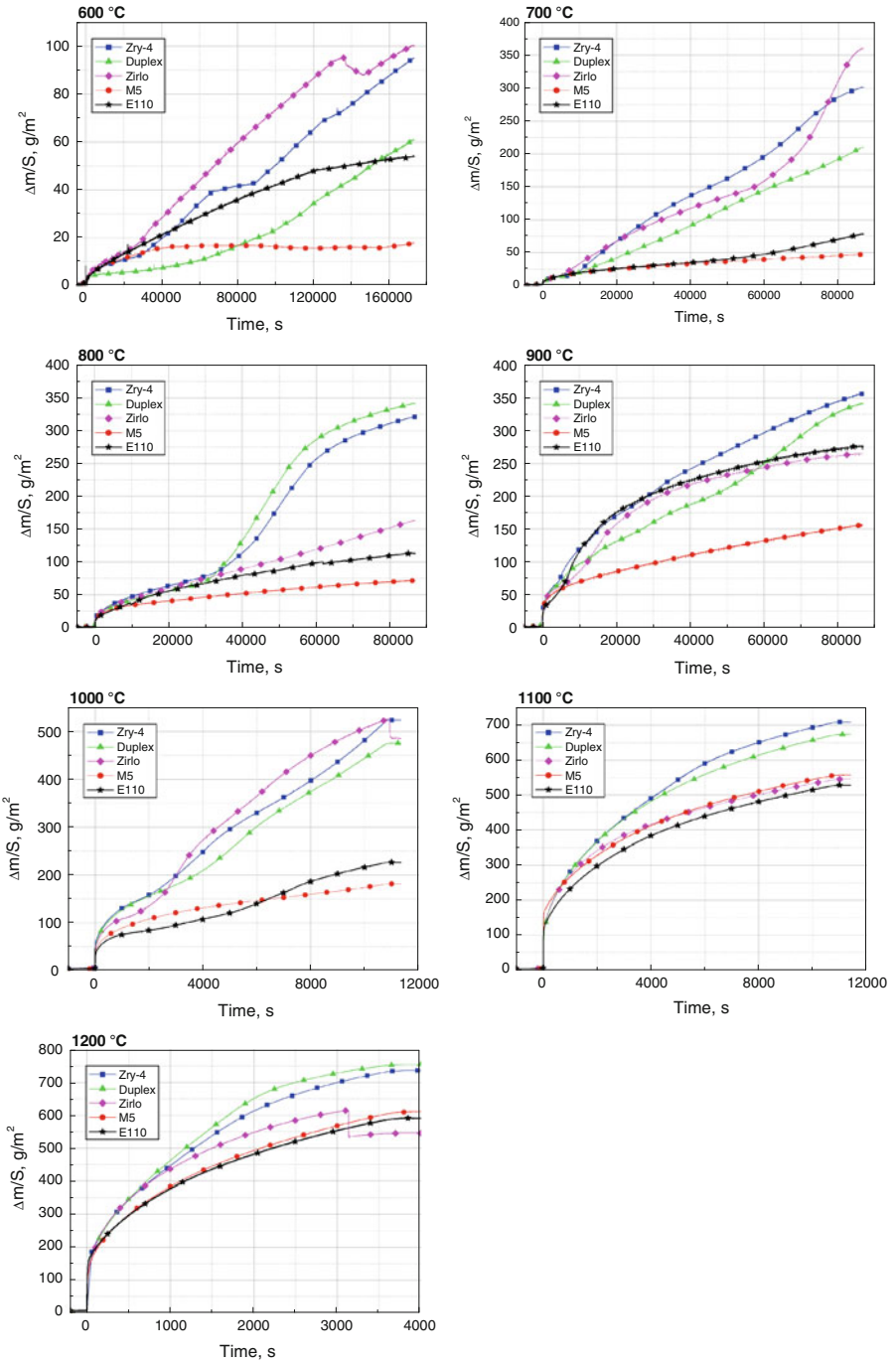

Fig. 2 Specific mass gain versus time during isothermal oxidation of zirconium alloys at 600–1200 °C in steam

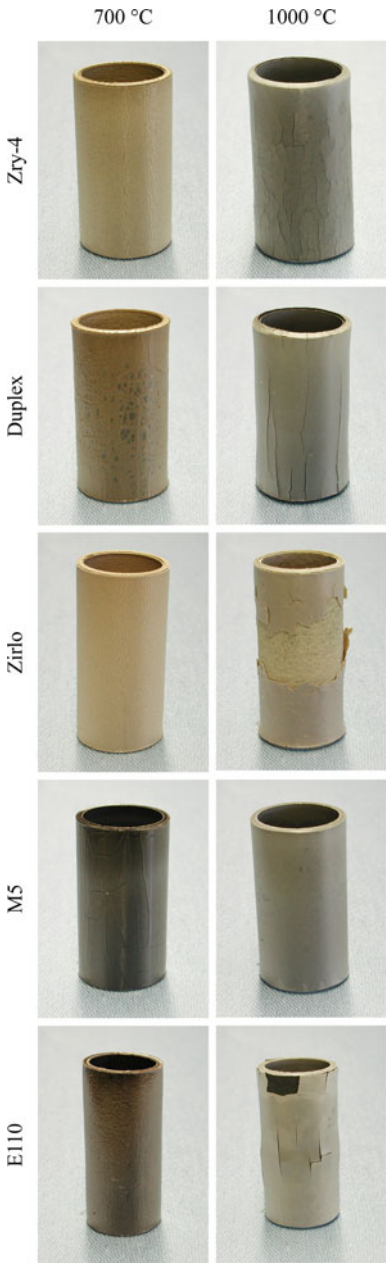

Fig. 3 Post-test appearance of zirconium alloy specimens after isothermal oxidation at 700 and 1000 °C in steam

The metallographic images compiled in Fig. 4 give a closer view into the thickness and structure of the oxide layers. They confirm the TG results. Pronounced breakaway oxidation is seen for Zry-4 and ZIRLO^{TM} at 700, 900, and 1000 °C and for E110 at 900 °C. The positive effect of the external low-tin layer at Duplex is visible on all specimens, but most pronounced at 700 and 900 °C.

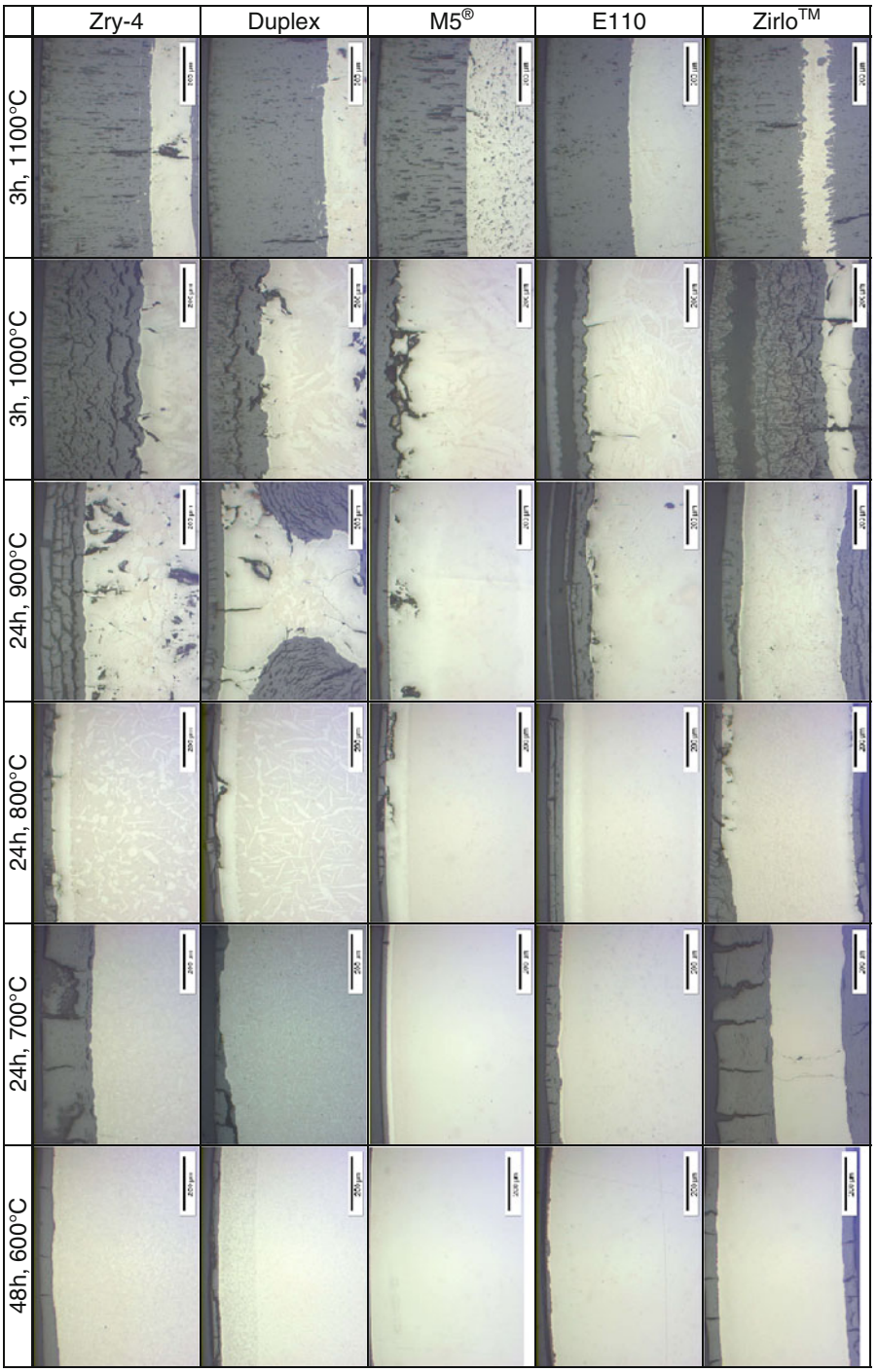

Fig. 4 Micro images of cladding cross sections after isothermal oxidation at 600–1100 °C in steam

The structure of the oxide scales after breakaway oxidation obtained at up to 1000 °C is characteristically very porous, layer-wise or with many peripheral cracks. The single oxide layers of the E110 cladding are thinner than those of the tin alloys. M5® shows no breakaway at all after all tests.

A closer view shows the external part of the oxide layer, which was formed first, differently from the bulk, due to its density. These external parts and the whole oxide scales formed at 1100 and 1200 °C exhibit columnar microstructures. Locally intensified oxidation is seen after some tests. The specimens of the 1200 °C tests looked similar to those oxidized at 1100 °C, but even more oxidized with only very thin metal layers remaining in the center of the tube segments. They were very brittle and partly broke during handling. The very wavy metal-oxide boundary of the ZIRLO™ specimens after the tests at 1100 and 1200 °C is noticeable. Furthermore, relatively thin and less degraded oxide scales of the 800 °C specimens (apart from local effects) are remarkable.

The end-of-test figures for the oxide, oxygen-stabilized α phase layer, and the remaining prior-β phase of all specimens are compiled in Table 2. Due to (partially local) breakaway oxidation, approximate values or ranges for the thickness of the individual phase had to be given. Generally, the oxygen-stabilized α-Zr(O) layers are very thin or even not visible in case of fast oxidation due to breakaway. They are comparably thick to the oxide scales or even thicker after slow oxidation through dense oxides which gives enough time for diffusion of oxygen into the metal phase.

Transient Tests in the Range of 600–1200 °C

The long-term isothermal tests resulted in breakaway oxidation with significantly accelerated kinetics for most of the alloys in the temperature range of up to 1000 °C. Therefore, the question arose if breakaway also plays a role during more prototypic transient oxidation with only limited time in the temperature window for breakaway.

The TG furnace allowed investigation of heating rates in the range 5–40 K/min. First, all specimens were investigated at the lowest heating rate. Figure 5 shows that only the TG curve of the E110 alloy has irregularities; these start at about 880 °C indicating spalling (and falling off) of oxide scales connected with a subsequent rise in reaction rate. As expected, all other curves continuously increase with temperature. Post-test inspection of the specimens gave no hints for breakaway oxidation either.

Faster heat-up with shorter times in the breakaway temperature window should decrease the likelihood of breakaway; so, only E110, and Zry-4 for comparison, were further investigated at higher heating rates. Strong deviations from “normal” TG curves are seen up to a heating rate of 10 K/min (Fig. 6), which is again indicative of spalling of oxide scales during oxidation. A closer look at the curves at 20–40 K/min shows also bends to faster oxidation rates caused by reduced diffusion resistance of the oxide layer. Post-test inspection confirmed the formation of loose oxides on these specimens (which fell off only post-test).

Table 2 End-of-test figures for oxide, oxygen-stabilized α phase, and β phase thicknesses in μm

Temp. (°C), time (h)	Layer	Zry-4	Duplex	M5	E110	Zirlo
600, 48	ZrO_2 outside	52	26	11	14	51
	ZrO_2 inside	59	49	13	11	49
	α outside	n.v.	n.v.	8–10	4–10	n.v.
	α inside	n.v.	n.v.	6–8	4–8	n.v.
	β	~650	~690	675	625	450–480
700, 24	ZrO_2 outside	185	20–90	20	40–70	210
	ZrO_2 inside	180	175	20	20–60	190
	α outside	2–10	~15	25	~10	n.v.
	α inside	2–10	10–20	25	~10	n.v.
	β	~500	550–600	635	~550	250–280
800, 24	ZrO_2 outside	~40	~30	22	~55	38; 50–130
	ZrO_2 inside	~45	~40	22	~60	37; 120
	α outside	60	60–65	75	75	60
	α inside	60	60–65	75	75	60
	β	550	560	515	430–450	350
900, 24	ZrO_2 outside	<170	~325 (75)	40	<85	70
	ZrO_2 inside	<225	~740	40	<105	<165
	α outside	~190	160–180	125–150	25–50	10–15
	α inside	~155	160–180	125–150	25–50	n.v.
	β	125	200	350–380	400–430	350–390
1000, 3	ZrO_2 outside	<380	<230	~75	~95	>260
	ZrO_2 inside	<340	<360	~55	~55	~355
	α outside	~95	100–120	100–125	60–80	85–130
	α inside	~65	75–90	100–125	60–80	
	β	~125	170–200	400–425	400–450	–
1100, 3	ZrO_2 outside	~455	~430	~385	320	~340
	ZrO_2 inside	~410	~395	~295	285	~345
	α outside	150–190	180–200	~300	275	100–120
	α inside					
	β	–	–	–	–	–

n.v. = not visible

Determination of Absorbed Hydrogen

The hydrogen content after isothermal oxidation of most of the specimens was determined by neutron radiography. Table 3 and Fig. 7 summarize the results. There is a clear difference between M5® on the one hand and Zry-4, Duplex, ZIRLO™, and E110 on the other hand. The hydrogen content increases with reaction temperature for the M5® alloy. All other alloys show maximum hydrogen contents at intermediate temperatures with highest values at 900 °C (E110) or 700 °C (Zry-4, Duplex, ZIRLO™). The absolute values of hydrogen concentration

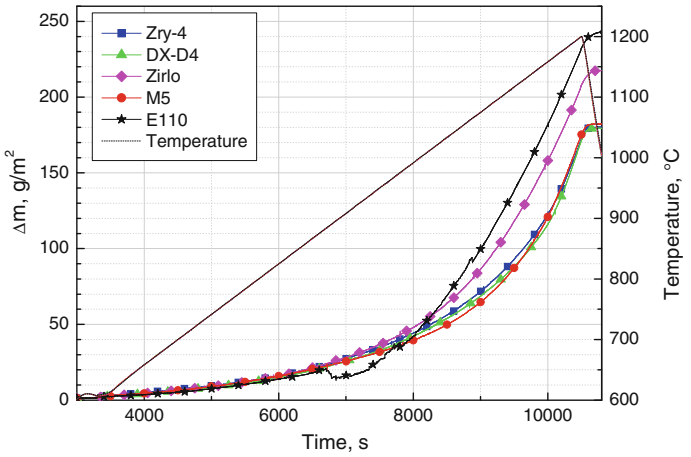

Fig. 5 Mass gains and temperatures during 5 K/min transient oxidation of Zr alloys in steam between 600 and 1200 °C

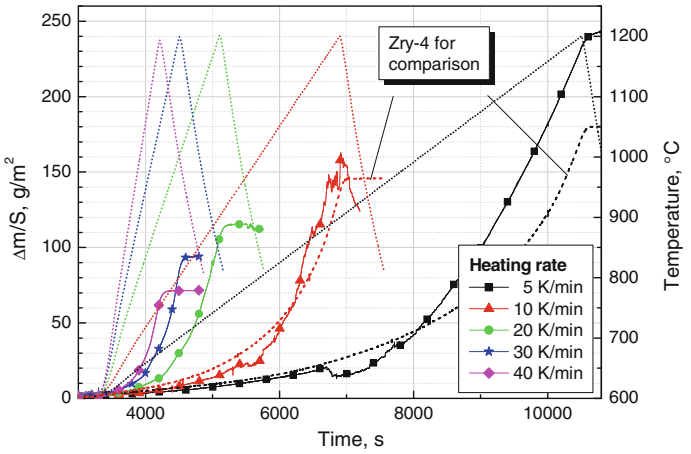

Fig. 6 Mass gains and temperatures during transient oxidation of E110 in steam between 600 and 1200 °C with heating rates varying between 5 and 40 K/min

Table 3 Hydrogen absorbed by zirconium alloys during isothermal oxidation in steam in at.%

T (°C)	t (h)	Zry-4	Duplex	Zirlo	M5	E110
600	48	22.40	14.44	10.85	0.07	4.82
700	24	39.15	34.35	36.08	0.95	4.35
800	24	–	–	8.00	0.79	12.65
900	24	–	24.58	18.80	2.46	24.68
1000	3	14.30	20.18	6.91	5.05	18.99
1100	3	11.28	14.52	7.29	12.51	13.62

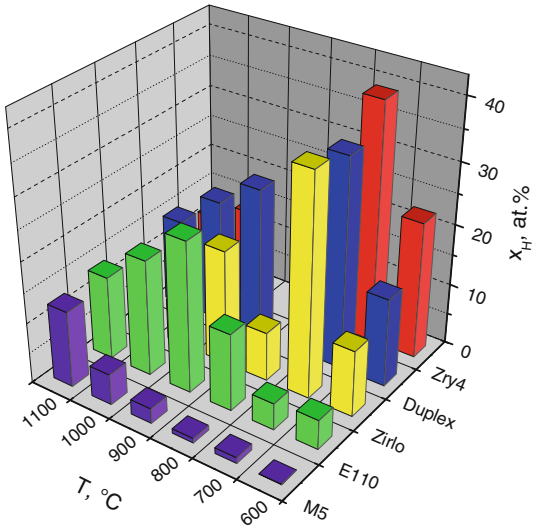

Fig. 7 Hydrogen absorbed by zirconium alloys during isothermal oxidation in steam in at.% (corresponding to the initial Zr mass)

with up to 40 at.% corresponding to more than 5000 wppm are high. The highest values correspond to a hydrogen uptake rate of more than 20%; i.e., more than 20% of the hydrogen produced during the oxidation reaction was absorbed by the remaining metal.

Discussion

The results presented in the previous chapter generally show complex oxidation kinetics and strong differences between the various zirconium alloys at up to 1000 °C and a more comparable behavior at higher temperatures. This contrast is due to the breakaway effect [8] which occurs during zirconium oxidation at up to approx. 1050 °C and which is caused by phase transition from meta-stable tetragonal to monoclinic ZrO_2 connected with a volume change of 10% in that temperature regime. The phase transition leads to the formation of circumferential cracks in the oxide scale and partial spalling and, therefore, to impairment or even loss of the protective effect of the oxide scale. The tetragonal oxide formed above 1050 °C is thermodynamically stable and is not susceptible to breakaway.

The kinetics of the oxidation of zirconium and its alloys can be described by the following equation:

$$\frac{\Delta m}{S} = k_m \cdot t^n \tag{1}$$

where Δm is the mass of oxygen absorbed by the specimen, S is the sample surface, k_m is the rate constant and t is the oxidation time at constant temperature. The exponent n equals ½ for the parabolic oxidation kinetics, applicable to a protective oxide scale at temperatures above 1000 °C. In this case, the oxidation rate is determined by the diffusion of oxygen through the oxide scale. At lower

temperatures, cubic or sub-cubic oxidation kinetics ($n = 1/3$ and $n < 1/3$, respectively) are observed, as e.g., described and explained by Evans [9]. When the oxide scale loses its protective effect, oxygen may be transported much faster through pores and cracks to the metal surface, thus accelerating the oxidation kinetics to linear ($n = 1$) or even faster.

Figure 2 indicates this general behavior at all temperatures ranging from 600 to 1000 °C. Generally, the transition is more abrupt for the tin alloys and more gradual for the niobium alloys. Figure 8 shows these transitions for 700 and 900 °C as examples in log–log diagrams more clearly.

Table 4 summarizes the results in terms of times of transition to breakaway and accelerated oxidation and with respect to oxide thickness at transition. In most cases, breakaway occurs after hours and should be of limited importance for reactor transients. Even the shortest transition times amount to more than half an hour. The high oxidation rates of the different alloys at the various temperatures correlate with early transition to breakaway oxidation. The ZrO_2 oxide scale thickness at transition increases with temperature due to the rising ductility of the oxide. At least at higher temperatures within the breakaway regime, the calculated values of critical oxide scale thickness confirm the visual impression of thinner breakaway oxide scales for E110. M5® shows (almost) no breakaway oxidation at all; only slight deviations from ideal oxidation kinetics, only determined by oxygen diffusion through the growing oxide layer, were observed.

The late transitions of E110 at 700 °C and of the tin-bearing alloys at 800 °C are remarkable and may be correlated to the properties of the metal phase. It is known that Zr alloys have a maximum ductility at the beginning of the α–β transition which is for Zry-4 at around 850 °C and for niobium-bearing alloys at slightly lower temperatures [10]. Oxygen, as an α-phase stabilizer, and hydrogen, as an β-phase-stabilizing element, influence this transition temperature; but probably there is a

Table 4 Transition times in seconds from protecting to non-protecting oxide scales (breakaway) and calculated oxide scale thickness at transition in μm *(italic)*

T (°C)	Zry-4	Duplex	Zirlo	M5	E110
600	29600	27700	22700	nt	nt
	7	*3*	*8*		
700	8080	8100	5110	nt	46800
	9	*9*	*9*		21
800	26800	26200	18800	nt	3310
	41	*35*	*32*		*12*
900	4610	4900	7490	nt	2810
	40	*38*	*40*		*24*
1000	2120	3364	2070	nt	2320
	89	*105*	*76*		*48*
1100	nt	nt	nt	nt	nt
1200					

nt–no transition

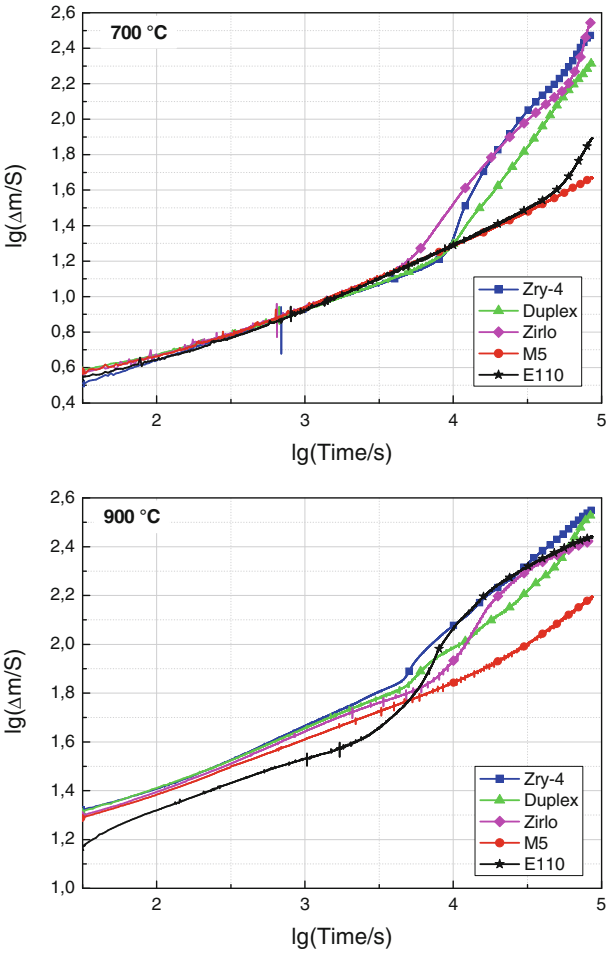

Fig. 8 Mass gain during oxidation of zirconium alloys in steam at 700 (*top*) and 900 °C (*bottom*)

correlation between the high ductility of the metal phase and the delay in transition to accelerated oxidation which is dependent on alloy composition.

The relatively early transition of E110 over a wide temperature range causes breakaway oxidation also under transient conditions as was already found in [3]. The critical oxide scale thickness at transition in the transient tests with E110 was 12–6 μm, respectively, with the lowest value for the highest heating rate. Obviously, for the other alloys the temperature window for breakaway is much smaller, giving not enough time for reaching the critical oxide thickness.

The significant difference between the two Zr–Nb alloys is due to the different fabrication procedures resulting in different impurities [11]. The zircon ore decomposition, hafnium purification processes, and electrolytic zirconium reduction for E110 raw material are based on fluorine chemistry. Fluorine is known to be deleterious leading to increased susceptibility to breakaway oxidation. On the other

Table 5 Parabolic rate constants in $gm^{-2}\ s^{-0.5}$ for oxidation of zirconium alloys in steam

T (°C)	Zry-4	Duplex	Zirlo	M5	E110
600	0.063	0.05	0.0894	0.0723	0.0813
700	0.201	0.14	0.177	0.167	0.156
800	0.394	0.34	0.349	0.307	0.244
900	0.966	0.55	0.843	0.377	0.420
1000	3.64	2.74	1.90	1.83	1.82
1100	6.69	6.47	5.87	4.61	4.77
1200	10.91	11.99	11.69	9.10	8.31

hand, M5® fabrication, as well as the production of other western cladding alloys, is based on processes leading to Ca, Mg, and Al impurities which are beneficial for the formation of oxide scales less susceptible to breakaway [11].

Although the oxidation kinetics are strongly influenced by breakaway and the oxidation kinetics up to 900 °C are rather cubic, it is reasonable to determine the parabolic rate constants for the pre-transition phase. Parabolic correlations are included in all accident simulation codes and breakaway is not expected during fast accident transients. Figure 9 shows that the data of this study reasonably correlate with the correlation by Cathcart and Pawel [12] for $T < 1550$ °C. The rate constants of the various alloys, also summarized in Table 5, differ by a maximum factor of three at 900 °C. The two Zr1Nb alloys M5® and E110 have almost identical rate constants over the whole temperature range investigated which are lowest at $T > 700$ °C. Zircaloy-4 and Duplex naturally behave in a very similar way with a slightly beneficial behavior of Duplex up to 1000 °C. (This effect would be more pronounced if only external oxidation were investigated.) At higher temperatures, the beneficial effect of the low-tin corrosion-optimized layer is reduced due to fast tin diffusion leading to increase of tin content in the external layer [3, 13]. The rate constants obtained by TG tests in this study correlate well with former own investigations [13] obtained in a horizontal tube furnace.

Figure 9 also shows the transition from low-temperature to high-temperature oxidation caused by the monoclinic-tetragonal phase transition in the oxide between 1000 and 1100 °C for ZIRLO™ and between 900 and 1000 °C for all other alloys.

The tight correlation between oxide morphology and hydrogen absorption, already discussed elsewhere [14] for integral bundle tests, is clearly confirmed by this study. Local enrichment of hydrogen in pores and cracks of the oxide layer leads to significantly higher hydrogen partial pressures than in the gas atmosphere and, therefore, according to Sieverts' law [15], to higher hydrogen concentrations in the metal phase ("hydrogen pump effect" [14]). High concentrations of hydrogen in the metal have been found in specimens with pronounced breakaway oxide scales, with the highest values for specimens with early transition times to breakaway. The hydrogen concentration in M5® alloy is monotonically dependent on temperature, indicating that here only hydrogen content in the gas bulk played a role and

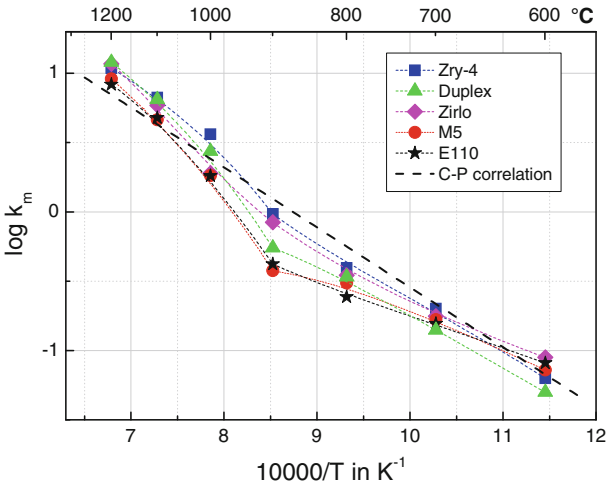

Fig. 9 Parabolic rate constants for the oxidation of zirconium alloys in steam. Up to 1273 K only pre-transition data were used for the fitting procedure. For comparison, the Cathcart–Pawel correlation [11] is shown

confirming the absence of layered oxide scales seen in the metallographic examination.

Generally, the oxidation of zirconium alloys is strongly dependent on composition and boundary conditions, like oxidizing atmosphere, as soon as breakaway starts. The comparison of the results of this study with recent studies in steam [3], oxygen [4], and air [16, 17] shows strong differences in oxidation behavior up to about 1050 °C. On the other hand, the pre-transition oxidation kinetics up to 1050 °C and the overall oxidation at higher temperatures are quite comparable and less dependent on composition and boundary conditions. A detailed analysis of the influence of the gas composition on oxidation will be the topic of a future paper and is beyond the scope of this one.

Summary and Conclusions

Four cladding materials used nowadays worldwide in pressurized water reactors, together with the classical Zircaloy-4 as the reference material have been investigated regarding their oxidation kinetics in flowing steam over a wide range of temperatures in isothermal and transient TG experiments. Differences in oxidation rates up to 800% were observed at temperatures up to 1000 °C. Smaller, but still significant variations (about 30%) were observed at higher temperatures. Generally, the advanced cladding alloys exhibit also a more favorable behavior at high temperatures typical of reactor accident scenarios.

The oxidation kinetics is determined by the growing superficial oxide scale, ideally leading to (sub-)parabolic rate law. For all alloys, except for M5®, more or less pronounced breakaway of the oxide scale leads to transition from these

(sub-)parabolic kinetics to linear or even faster ones at temperatures below 1050 °C after a certain time.

Breakaway plays no role for most of the alloys during even slow temperature transients. Therefore, parabolic rate constants obtained for the pre-transition period can be used in computer codes simulating accident sequences. Separate correlations for the different cladding alloys should be used because they differ by up to a factor of three in the intermediate temperature range. One example of the positive effect of using appropriate correlations is given in [18]. Otherwise, breakaway oxidation has to be considered for all scenarios with long durations at temperatures between 600 and 1050 °C like e.g., in spent fuel pool accidents or for analysis of the Paks cleaning tank incident [19].

Furthermore, a strong correlation between morphology of oxide scales and hydrogen uptake was confirmed. Both, oxygen and hydrogen uptake, lead to embrittlement of the cladding alloys and have to be taken into account for corresponding evaluations of the stability of claddings.

Further studies on the mechanism of breakaway and the influence of boundary conditions are envisaged. Additionally, the QUENCH-ACM program [6], conducted at KIT with 21–31 fuel rod simulator bundles with advanced cladding alloys, has complemented these investigations.

Acknowledgments This work was sponsored by the HGF Program NUKLEAR at the Karlsruhe Institute of Technology and partially done within the framework of the SARNET Mobility Program (contract FI6O-CT-2004-509065). The authors are very grateful to P. Severloh and U. Stegmaier (KIT) for sample preparation and microscopic examinations, as well as to C. Vorpahl for performing a number of TG tests. We also thank Tim Haste (IRSN) for his thorough review of the paper. The Zr1Nb (E110) was provided by Russian institutions in the context of the EU program ISTC 1648.2. M5® and Duplex-D4 rod cladding were delivered by AREVA, ZIRLO™ by Westinghouse.

References

1. B. Cox, *Journal of Nuclear Materials* **336**, 331 (2005).
2. G. Schanz, B. Adroguer, and A. Volchek, *Nuclear Engineering and Design* **232**, 75 (2004).
3. M. Grosse, *Nuclear Technology* **170**, 272 (2010).
4. M. Steinbrück, *Oxidation of Metals* **70**, 317 (2008).
5. M. Steinbrück, *The Nuclear Materials Conference NuMat 2010, 4–7 October 2010,* (Karlsruhe, Germany, 2010) (to be published in Journal of Nuclear Materials).
6. L. Sepold, M. Grosse, M. Steinbrück, and J. Stuckert, *16th International Conference on Nuclear Engineering, May 11–15, 2008* (Orlando, FL, USA, 2008) (paper ICONE16-48074).
7. M. Grosse, E. Lehmann, P. Vontobel, and M. Steinbrueck, *Nuclear Instruments and Methods in Physics Research Section A* **566**, 739 (2006).
8. G. Schanz, *Report FZKA-7329* (Forschungszentrum Karlsruhe, 2007).
9. H. E. Evans, D. J. Norfolk, and T. Swan, *Journal of the Electrochemical Society* **125**, 1180 (1978).
10. T. Forgeron et al., *Zirconium in the Nuclear Industry: Twelfth International Symposium,* eds. G. P. Sabol and G. D. Moan, ASTM STP1354 (West Conshohocken, PA, 2000), p. 256.
11. H. M. Chung, *Nuclear Engineering and Design* **37**, 327 (2005).
12. J. V. Cathcart et al., *ORNL/NUREG-17* (1977).
13. M. Grosse and R. Simon, *Advanced Engineering Materials* **11**, 483 (2009).
14. M. Grosse, E. Lehmann, M. Steinbrück, G. Kühne, and J. Stuckert, *Journal of Nuclear Materials* **385**, 339 (2009).
15. M. Steinbrück, *Journal of Nuclear Materials* **334**, 58 (2004).

16. C. Duriez, M. Steinbrück, D. Ohai, T. Meleg, J. Birchley, and T. Haste, *Nuclear Engineering and Design* **239**, 244 (2009).
17. M. Steinbrück, *Journal of Nuclear Materials* **392**, 531 (2009).
18. J. Birchley, T. Haste, and B. Jäckel, *Proceedings. of the 14th Internation QUENCH Workshop, 4–6 November 2008,* ed. M. Steinbrück, ISBN 978-3-923704-67-5 (Forschungszentrum Karlsruhe, Germany, 2008).
19. Z. Hozer, M. Horvath, M. Kunstar, L. Matus, I. Nagy, T. Novotny, E. Perez-Fero, A. Pinter-Csordas, N. Ver, A. Vimi, and P. Windberg, *Nuclear Engineering and Design* **241**, 573 (2011).